

Synthesis and Biological Investigation of (+)-JD1, an Organometallic BET Bromodomain Inhibitor.

Storm Hassell-Hart,[†] Andrew Runcie,[#] Tobias Krojer,[‡] Jordan Doyle,[†] Ella Lineham,[‡] Cory Ocasio,[†] Brenno A. D. Neto,^Ω Oleg Fedorov,[‡] Graham Marsh,[^] Hannah Maple,[^] Robert Felix,[^] Rebecca Banks,[^] Alessio Ciulli,[#] Sarah Picaud,[‡] Panagis Filippakopoulos,[‡] Frank von Delft,[≈] Paul Brennan,[‡] Helen J. S. Stewart,[¢] Timothy J. Chevassut,[¢] Martin Walker,[∞] Carol Austin,[∞] Simon Morley,[‡] John Spencer.^{†*}

[†]Chemistry Dept, School of Life Sciences, University of Sussex, BN1 9QJ, UK.

[#]Division of Biological Chemistry and Drug Discovery, School of Life Sciences, University of Dundee, James Black Centre, Dow Street, Dundee DD1 5EH, Scotland, U.K.

[‡]Structural Genomics Consortium (SGC), University of Oxford, Oxford OX3 7DQ, UK.

[‡] Biochemistry Department, School of Life Sciences, University of Sussex, BN19QQ, UK.

^ΩLaboratory of Medicinal and Technological Chemistry, University of Brasília, Chemistry Institute (IQ-UnB), Campus Universitário Darcy Ribeiro, Brasília, Q3 Distrito Federal, 70904-970, Brazil.

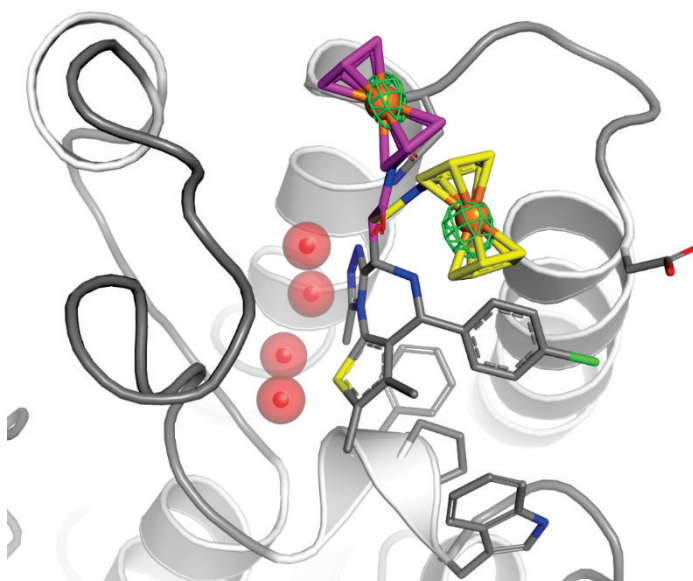
[^]Tocris Bioscience, the Watkins Building, Atlantic Road, Avonmouth, Bristol BS11 9QD, U.K.

[∞]Eurofins Selcia Drug Discovery, Fyfield Business & Research Park, Fyfield Road, Ongar, Essex CM5 0GS

[≈]Diamond Light Source (DLS), Harwell Science and Innovation Campus, Didcot, OX11 0DE, UK.

[¢] Brighton and Sussex Medical School, University of Sussex, Brighton, BN1 9PS, UK.

ABSTRACT. (+)-JD1, a rationally designed ferrocene analogue of the BET bromodomain (BRD) probe molecule (+)-JQ1, has been synthesized and evaluated in biophysical, cell based assays as well as in pharmacokinetic studies. It displays nM activity against BRD isoforms and its cocrystal structure was determined in complex with the first bromodomain of BRD4 and compared with that of (+)-JQ1, a known BRD4 small molecule probe. At 1 μ M concentration, (+)-JD1 was able to inhibit c-Myc, a key driver in cancer and an indirect target of BRD4.



INTRODUCTION.

The study of post translational modifications (PTMs) remains a field of intense activity in epigenetics. Bromodomains (BRDs) are acetylated lysine (KAc) evolutionary conserved reader modules and are indispensable in the “write-erase-read” epigenetic code driving gene transcription and silencing.¹ BRDs directly impact upon, *inter alia*, a number of cancers and inflammation processes.^{2,3,4,5} The BET bromodomain family (bromodomain and extra-terminal) comprises four proteins, namely bromodomain-containing proteins 2 - 4 (BRD2, BRD3, BRD4) and bromodomain testis-specific protein (BRDT) with each member containing two tandem N-terminal bromodomains and an extra-terminal protein interaction domain (ET). Important anchoring sites for the KAc motif are provided by conserved asparagine and tyrosine residues, the latter via a hydrogen bond to one of four structural water molecules.^{6,7}

Out of the 61 BRDs in humans, BRD4 is undoubtedly the most studied, with notable progress in the development of probe molecules and clinical candidates, which include TEN-010, OTX015, I-BET762 and the thienodiazepine (+)-JQ1 (Figure 1).^{8,9} The latter was shown to be a potent inhibitor of BRD4(1), and its co-crystal structure in BRD4(1) showed it to occupy the KAc binding pocket via a hydrogen bond formed between the methyltriazole unit and Asn140.¹⁰

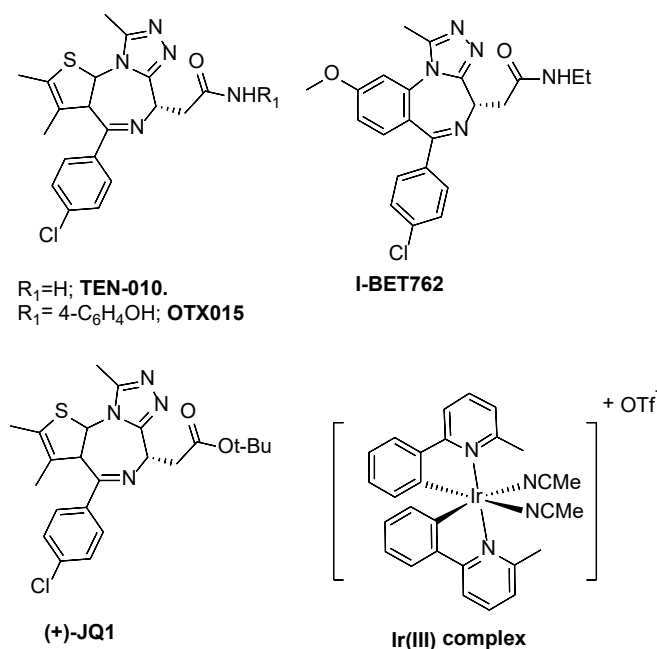


Figure 1. Representative BRD4 Inhibitors.

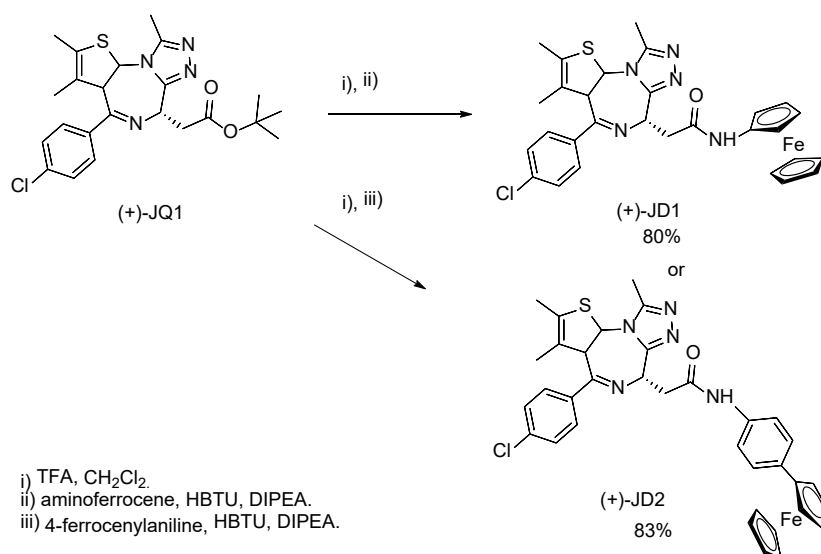
The incorporation of transition metal complexes into bioactive molecules can improve ligand exchange processes and pharmacokinetics,^{11,12} and enable redox behavior due to several accessible oxidation states.¹³ Moreover, it can lead to enhanced steric and hydrophobic interactions with the target protein, especially with bound ligands such as cyclopentadienyl,¹⁴ and to increased coordination numbers such as octahedral geometry (termed “hypervalent carbon”), beyond tetrahedral carbon.^{15,16,17,18,19}

Recent studies, based on screening a library of around 30 octahedral metal complexes, revealed an iridium complex (**Ir(III)**, Figure 1)²⁰ with comparable in vitro BRD4 binding to (+)-JQ1 and antiproliferative in vivo activity when dosed at 100 mg/kg. In the current case, we present a rationally-designed metal-containing BRD4 inhibitor where we reasoned that the BET BRD inhibitor (+)-JQ1, described above, might be receptive to incorporation of an aminoferrocene bioisostere to replace the t-Bu ester group (PDB; 3MXF).^{21,22,23,24,25,26,27} We describe herein the synthesis of organometallic complexes related to (+)-JQ1, and their biological and pharmacokinetic evaluation.

RESULTS AND DISCUSSION

After deprotection of commercially available (+)-JQ1, standard coupling chemistry led to the ferrocene-substituted amide analogues (+)-JD1 and (+)-JD2, which were characterized by ¹H and ¹³C NMR spectroscopy and were >95% pure by HPLC and by chiral HPLC (Scheme 1). This was verified by the synthesis of (-)- or racemic JD1 and JD2 as HPLC and assay controls (Figure S5-10).

Scheme 1. Synthesis of (+)-JD1 and (+)-JD2.



A co-crystal structure determination of (+)-JD1 in complex with the first BRD of BRD4 was performed (Figure 2 (a)). From the (+)-JQ1 structure (Figure 2 (c); see PDB; 3MXF), the t-butyl ester substituent nestles into the small depression created by the side-chains of Leu92 and Leu94. The interaction is quite tight and as a result, there is no space for a water molecule to interact with the alkoxy group although the ester carbonyl group forms H-bonds with well-defined water molecules around it. The electron density map for the ferrocene group of (+)-JD1 was initially ambiguous. An anomalous difference Fourier map from data collected just below the Fe K-edge showed two peaks with an r.m.s. density of 8.9 and 7.5, respectively. Hence, the ferrocene moiety was modelled in two conformations with occupancies of 0.66 (yellow) and 0.34 (magenta), respectively (Figure S11). The B-factors for the ((+)-JQ1-like) core of (+)-JD1 are similar to the surrounding protein residues. However, they, unsurprisingly, go up towards the ferrocene group. Both (+)-JQ1 and (+)-JD1 form hydrogen bonds with surrounding water molecules although the carbonyl group of (+)-JD1 points into the opposite direction to the one in (+)-JQ1 (Figure 2(c)). We anticipated that (+)-JD1 would be less potent, due to the different conformations adopted, than (+)-JQ1.

With the new complexes to hand, we next looked to evaluate them biologically. (+)-JD1 and (+)-JD2 were titrated, alongside (+)-JQ1, against all somatic human BET bromodomains (BRD 2-4, BD1, BD2) in an AlphaLISA assay, which measures the displacement of a biotinylated JQ1 analogue, Bio-JQ1^{28,29} using a modification of a known procedure.³⁰ In general, mean pIC₅₀ values (negative log of the IC₅₀ value, converted to molar; the corresponding respective IC₅₀ values are given in parentheses) were obtained with (+)-JQ1 = 7.0 (150 nM) compared with (+)-JD1 = 6.5 (400 nM), signifying a drop in potency of 0.5 log units (~3x loss). (+)-JD2 was only able to reach ~75% inhibition within our titrations and was visibly less potent against the BET BDs than (+)-JD1. IC₅₀ curves were fitted to the (+)-JD2 data assuming an I_{MAX} of 100%, giving a mean pIC₅₀ of 6.2 (750 nM) and a pIC₅₀ of 0.8 (~6.5x loss), although these values cannot be considered as reliable as those for (+)-JQ1 and (+)-JD1.

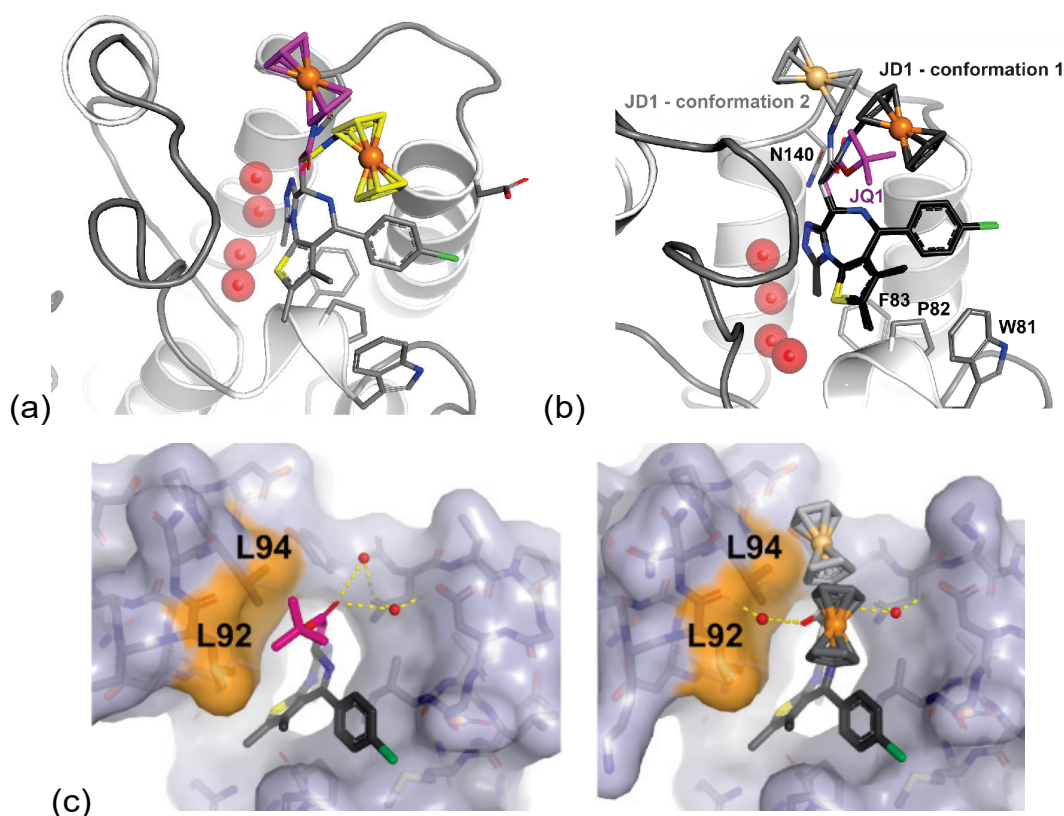


Figure 2. (a) Cocystal structure of (+)-JD1 in BRD4(1) showing two conformations of the ferrocene unit. (b) Superimposition of (+)-JD1 and (+)-JQ1. (c) Close-up of (+)-JQ1 (LHS) and (+)-JD1 (RHS) showing change of orientation of carbonyl group on moving from an ester to an amide.

As a negative control, like (-)-JQ1, the (-)- enantiomer of JD1 was shown to have little biological activity. When tested against BRD4 BD1 in the AlphaLISA assay, no significant inhibition was seen below 10 μM (Fig 3 (c)).^{31,32}

Since (+)-JD1 was found to be more potent than (+)-JD2, it was tested head to head with (+)-JQ1, in cell viability assays in several cancer cell lines. (+)-JQ1 exhibited nanomolar activity against all cell lines tested, whereas (+)-JD1 displayed micromolar potency against a triple negative breast cancer (TNBC) cell line (BT-549) and a prostate cancer cell line (LNCaP), with IC_{50} values of 9.9 μM and 5.2 μM , respectively (Figure 3(d)). Both (+)-JD1 and (+)-JQ1 showed the highest cell killing activity against the acute myeloid leukaemia (AML) cell line (MV-4-11), with IC_{50} values of 230 nM and 90 nM, respectively. This drop in cellular potency is slightly higher than the drop in AlphaLISA potency (ca. 6x versus 3x).

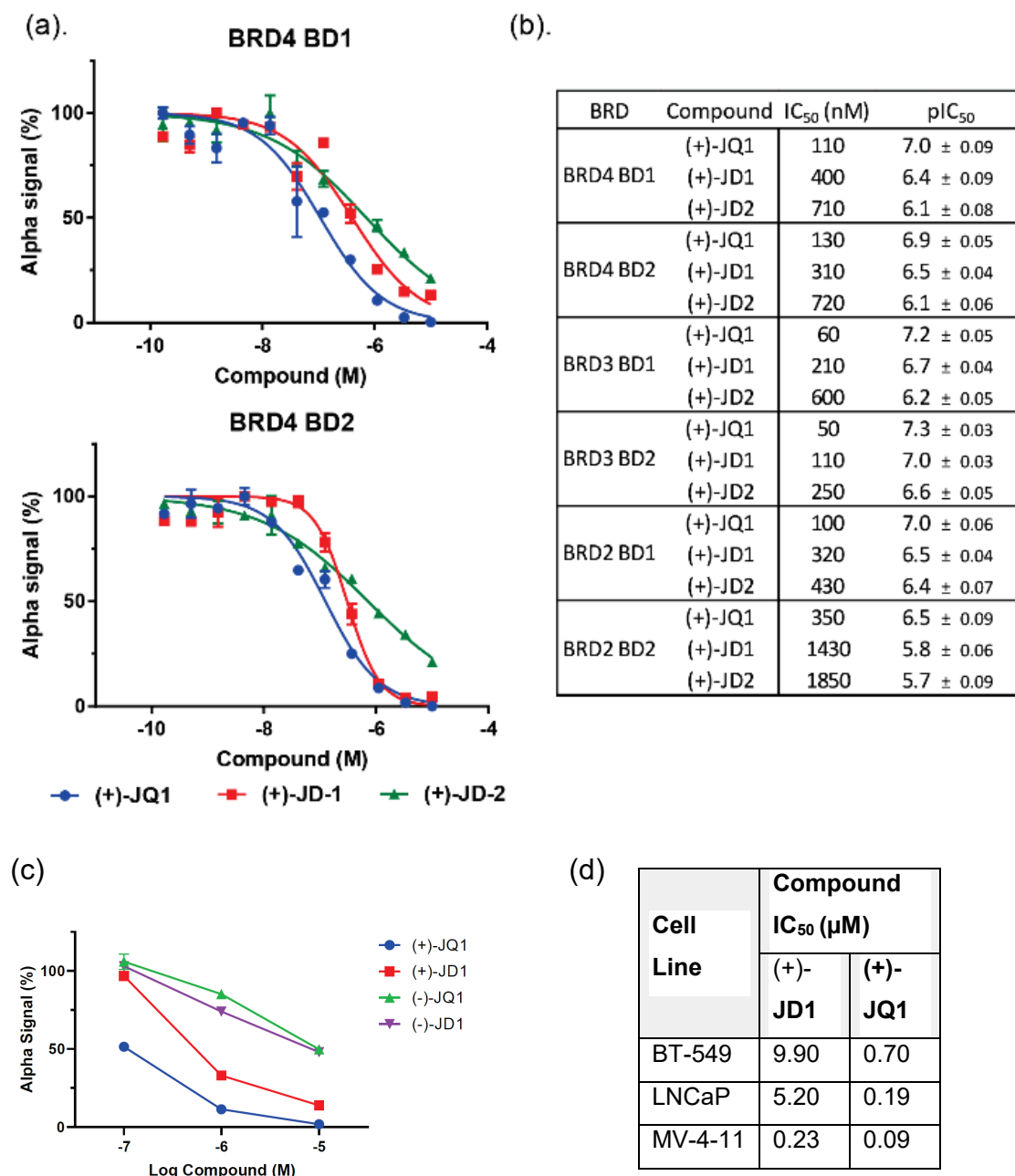


Figure 3. (a) Titration of (+)-JQ1, (+)-JD1 and (+)-JD2 against BRD4(1) and (2) in AlphaLISA assay. Data shown as mean ± S.E. of 2 replicate wells (b) IC₅₀ and pIC₅₀ (±SE) values for titrations against all somatic BET BDs. (b) IC₅₀ and pIC₅₀ (±SE) values for titrations against all somatic BET BDs. (c) AlphaLISA BRD4(1) assay for (-)-JQ1, (-)-JD1. (d) Cell viability with (+)-JQ1 or (+)-JD1 treatment. Average IC₅₀ of n=3. Data shown as mean ± S.D of triplicate wells.

Previous work in our laboratory investigated the redox pharmacology of a novel ferrocene-containing HDAC inhibitor, Pojamide,³³ on colorectal cancer cells (HCT116). This study utilised sodium nitroprusside (SNP), a known NO⁺ donor, to induce the formation of a ferrocenium species

and concluded that this led to enhanced DNA damage and cellular cytotoxicity in this cell line. Therefore, the redox properties and cytotoxicity of (+)-JD1 and its purported ferrocenium analogue (+)-JD1⁺, under similar conditions, were investigated in the cell line, MV-4-11, (Figure 3(c)), using a CellTiter-Blue assay (Promega). The addition of SNP at 25 μ M concentration, alone, had no effect on cell viability, as shown previously by our group by titration studies, MV-4-11 cells were then incubated for 72 h in the absence or presence of 100 nM (+)-JD1 or (+)-JQ1, and in the presence or absence of SNP and glutathione (GSH), which, was added in excess, as previously optimized, to eliminate SNP-induced toxicity (Figure 4(b)). As expected, (+)-JQ1 decreased cell viability to a greater extent than (+)-JD1 when tested as a single agent. The addition of SNP/GSH in conjunction with (+)-JQ1 had no significant effect on cell viability in comparison to (+)-JQ1 alone. However, when SNP/GSH were added to (+)-JD1, there was a slight decrease in cell viability (by ~10%) relative to (+)-JD1 alone. Although the reduction in cell viability was subtle, these data support the proposed model for the dual activity of (+)-JD1, dependent on the oxidation state of the iron atom in the ferrocene moiety. Attempts to independently synthesize and isolate (+)-JD1⁺ were unsuccessful suggesting its generation in cells is less favorable compared with its corresponding Pojamide Fe(III) species.

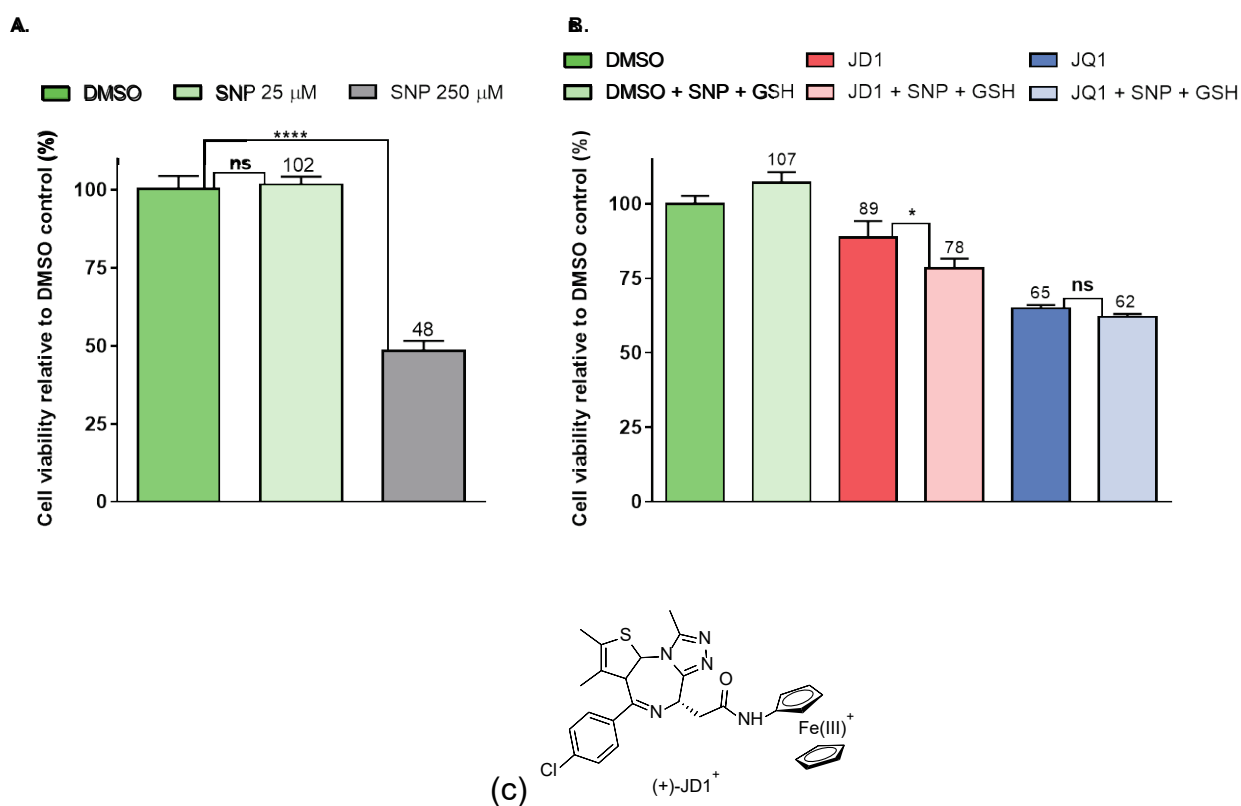
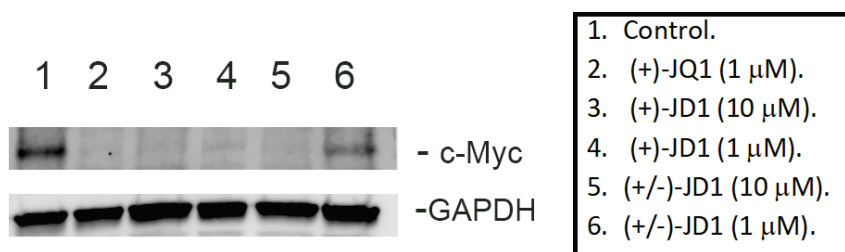
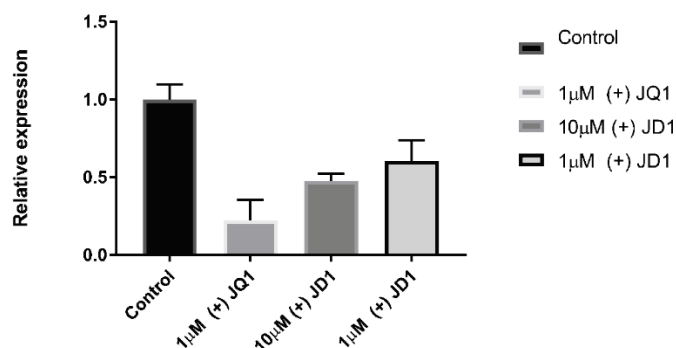


Figure 4. Cell viability of (+)-JD1 and (+)-JQ1 +/- 25 μ M sodium nitroprusside (SNP) on MV-4-11 cells. (a). Data are presented as the means \pm SD, n=3 (ns: non-significant and ****p \leq 0.0001 relative to DMSO). (b). Cells were treated for 72 hours with either 100 nM (+)-JD1 or 100 nM (+)-JQ1 +/- 25 μ M SNP/ 1 mM glutathione (GSH). (c) Structure of postulated (+)-JD1⁺.

The inhibition of BET bromodomains is a known indirect strategy to inhibit c-Myc, a key driver of cancer, which enables cancer cell survival and division³⁴. We, therefore, compared the expression of c-Myc in the presence of (+)-JQ1 and (+)-JD1 with ((+/-)) *rac*-JD1 as a negative control. (+)-JD1 was able to inhibit c-Myc expression down to 1 μ M concentration, comparable to that of (+)-JQ1, whereas incomplete inhibition was seen with (racemic) (+/-)-JD1 at this concentration, undoubtedly due to the presence of the inactive (-)-JD1 (Figure 5(a)). qRT-PCR (quantitative real time PCR) was performed on total RNA from cultures treated for 16 h with (+)-JQ1 or (+)-JD1 using c-Myc GAPDH as a housekeeping gene. Relative gene expression was normalised to GAPDH, and determined by the $2^{-\Delta\Delta C_t}$ method as previously described by our group.³⁵ This showed that (+)-JQ1, at 500 nM concentration, was vastly superior to (+)-JD1, even at 10 μ M concentration.



(a)



(b)

Figure 5. (a) Western blot of (+)-JQ1 and (+)-JD1 with *rac*-JD1 vs. c-Myc.(b) Total mRNA by qRT-PCR in the presence of (+)-JQ1 and (+)-JD1.

Finally, we evaluated the pharmacokinetic (PK) properties of (+)-JD1 vs. (+)-JQ1 in selected standard assays (Table 1).³⁶ Mouse microsomal metabolism of (+)-JD1 was extremely high with a clearance value *ca.* seven times that of (+)-JQ1. This metabolism is likely to be due to the formation of hydroxylated products (Figure S14). Both compounds had unfavourable plasma protein binding.

Table 1. Selected PK Properties of (+)-JD1.

Compound	Solubility cut-off (μ M):	Half-life (min)	CLint (μ l/min/mg protein) ^a	% Bound PPB ^a
Pyrene	10<x<25	nd	nd	nd
Aspirin	>100	nd	nd	nd
Verapamil	nt	12.5	111	89.3
(+)-JD1	10<x<25	2.6	533	>99.9
(+)-JQ1	>100	18.7	74	98.8

nt; not tested. Nd not determined.^a in mouse.

CONCLUSIONS.

The rationally designed bromodomain inhibitor (+)-JD1 has been synthesized in high yield. It displayed excellent BRD affinity in biochemical assays, albeit weaker than that of (+)-JQ1, which was rationalized by its X-ray co-crystal structure and suboptimal binding to BRD4(1), where two distinct ferrocene conformations were determined. A further slight increase in cell potency was observed when (+)-JD1 was converted to a purported Fe(III) species in cells after treatment with SNP. The high rate of metabolism of (+)-JD1 calls for a more general study of metabolism in metal containing compounds, which may improve their application in clinical settings.^{37,38} Further studies on metal-based BRD inhibitors are underway in our laboratory.

EXPERIMENTAL.

Solvents were used as purchased including deuterated solvents for NMR use. NMR spectra were recorded on a Varian NMR 400 (^1H 399.5 MHz; $^{13}\text{C}\{^1\text{H}\}$ 100.5 MHz or 500 (^1H 499.9 MHz; $^{13}\text{C}\{^1\text{H}\}$ 125.7 MHz). Chemical shifts are reported in ppm. Spectra are referenced to the corresponding protic solvent (^1H) or signals of the solvent (^{13}C). The progress of reactions was monitored by thin layer chromatography (TLC) using commercially available glass silica gel plates (60 Å, F254). The mobile phase was usually a solvent mixture and the visualization was undertaken using UV light. Chromatographic purifications were carried out on an ISCO Combi Flash RF 75 or 150 PSI purification unit, gel columns. LC-MS purity analyses were undertaken using a 5 μm C18 110 Å column. Percentage purities were performed using a 30 min method in water/acetonitrile with 0.1% formic acid (5 min at 5%, 5–95% over 20 min, 5 min at 95%) with the UV set to 254 nm. High-resolution mass spectrometry were carried out at the University of Sussex, as described elsewhere.

AlphaLISA.

AlphaLISA assays were carried out in 384-well, light-grey Alphasplates (PerkinElmer), with a final assay volume of 25 μl . Each assay component was diluted in AlphaLISA buffer (50 mM HEPES, 100 mM NaCl, 0.1% BSA, 0.02% CHAPS, pH7.5) to 5x its intended final concentration, and added at a volume of 5 μl , using a 12-channel Matrix P125 multi-channel pipette (Thermo). His-tagged protein, biotinylated (+)-JQ1 and test compounds were added to the well, and incubated for 1 h at room temperature. Then, in low-light conditions, Ni^+ chelator AlphaLISA acceptor beads (PerkinElmer) were added and incubated for 1 h, then Streptavidin-conjugated AlphaScreen donor beads (PerkinElmer) were added and incubated for 1 h. Alpha signal was measured in a Pherastar FS, using the AlphaLISA module. Dose-response curves were generated in Prism 6 (Graphpad). Final concentrations are as follows: 100 nM his-tagged BRD, 5 nM Bio-JQ1, 1% DMSO, 10 $\mu\text{g}/\text{ml}$ each bead.

Cell viability.

Cell viability was measured using the CellTiter-Glo 2.0 assay (Promega). The BET-dependent, AML cell-line MV4-11 was obtained from DSMZ, and cultivated in RPMI medium (Gibco) supplemented with 10% FBS and 1% L-glutamate (Gibco). Cells were kept in an incubator at 37°C, 5% CO_2 . MV4-11 cells were diluted in media to 2X the desired final concentration, and dispensed into a sterile, white, clear-bottomed 384-well cell-culture microplate (Greiner Bio-one)

at a volume of 25 μ l. Following 24 h incubation test compounds were serially diluted in media to 2x their desired final concentration, and added to the assay plate at a volume of 25 μ l. After 48 h incubation the assay plate was moved to room temperature for 30 minutes, then CellTiter-Glo 2.0 reagent was added to each well at a volume of 25 μ l. Following a 20 minute incubation the luminescence signal was read on a Pherastar FS (BMG). Dose-response curves were generated in Prism 6 (Graphpad). Final assay concentrations are as follows: 3×10^5 cells/ml, 0.05% DMSO, 5 μ M and below test compound.

Cell culture.

Breast cancer cell line BT-549 was sourced from the American Type Culture Collection (ATCC, Manassas, VA, USA), US. The human AML cell line MV4-11 was purchased from the German Collection of Microorganisms Cell Cultures (DSMZ, Braunschweig, Germany). The human prostate cancer cell line LNCaP was kindly donated by the Genome Damage and Stability Centre (GDSC) at the University of Sussex. Cell lines were maintained in Minimal Essential Medium with Glutamax and Earl's salts (MEM, Gibco) or RPMI medium (Gibco) and supplemented with 10% (v/v) foetal bovine serum (FBS, Pan Biotech) at 37°C in a humidified atmosphere with 5% CO₂.

Cell viability.

To assess cell viability in vitro, all cell lines were seeded into 96-well plates at various cell densities per 100 μ L media, then treated with 0.2% (v/v) DMSO or varying concentrations of compounds for 72 hr. Cell viability was measured using the CellTiter-Blue reagent (Promega, Madison, WI, USA) with fluorescence recorded at 560Ex/590Em using a Synergy HT Multi-Detection Reader (BioTek, Winooski, VT, USA). Relative cell viability at a given inhibitor concentration was determined by comparing the fluorescence to that of DMSO treated cells. Dose-response curves were generated in Prism 6 (Graphpad).

Purification and crystallization.

The first bromodomain of human BRD4 (BRD4(1)) was expressed and purified as described previously.⁸ Prior to crystallization, 3 μ L of 100 mM JD1 in DMSO were mixed with 100 μ L 6.4 mg/mL BRD4(1) and incubated for 2 hours at 4 °C. BRD4(1) in complex with JD1 was crystallized using the vapour-diffusion technique in 150 nL sitting drops containing 75 nL BRD4(1)-JD1 and 75 nL of a reservoir solution containing 60% MPD, 0.1M MIB pH 8.0 at 4 °C.

Data collection and structure solution

Prior to data collection, crystals were flash frozen in liquid nitrogen without addition of an additional cryo-protectant. A single-crystal dataset was collected on beamline I03 at the Diamond Light Source at a wavelength of 0.9762 Å. Data were integrated with XDS³⁹ and scaled with AIMLESS⁴⁰ up to a resolution of 1.38 Å as part of the XIA2 auto-processing pipeline⁴¹. BRD4(1)-JD1 crystallized in space group $P2_12_12_1$ with unit cell dimensions $a = 37.52\text{\AA}$, $b = 43.97\text{\AA}$, $c = 79.02\text{\AA}$, $\alpha = \beta = \gamma = 90^\circ$, which is similar to previously published BRD4(1) crystal structures. Initial refinement and map calculation was carried out with DIMPLE⁴² using a ligand-free version of BRD4(1) (PDB ID 3MXF) as starting model. The resulting model had an Rcryst/ Rfree of 22.1/ 26.1%, and the electron density map showed a strong signal for a bound JD1 molecule. Phenix.elbow⁴³ was used to generate ligand restraints for JD1. Restraints for the ferrocene moiety were manually adjusted using the geometry of the ferrocene group present in PDB ID 1A3L as a template. Likelihood-weighted 2mFo-DFcalc and mFo-DFCalc maps allowed unambiguous modelling of the thienotriazolodiazepine core of JD1, but the orientation and location of the ferrocene group remained ambiguous.

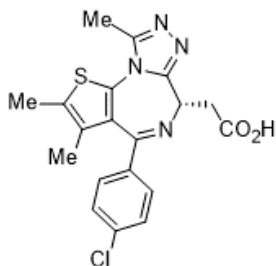
A second dataset from the same crystal was collected on beamline I04 at the Diamond Light Source at a wavelength of 1.7384 Å, just below the Fe K-edge, with the aim of using the anomalous signal of Fe to locate the position of the iron atom of the ferrocene group. Model phases from initial refinement and the measured anomalous differences were used as input and the resulting anomalous difference Fourier map displayed two outstanding peaks with an r.m.s. density of 8.9 and 7.5, respectively, in the ambiguous region. The ferrocene moiety was modelled in two conformations with occupancies of 0.66 and 0.34, respectively.

After several rounds of manual rebuilding in COOT⁴⁴ and subsequent cycles of refinement with REFMAC5⁴⁰, Rcryst/ Rfree of 14.9% and 17.9%, respectively. The model and structure factors were deposited in the Protein Data Bank (PDB) under accession number 6SE4.

Raw diffraction images of both datasets and ligand restraints for JD1 are available at the ZENODO data repository (10.5281/zenodo.3063129).

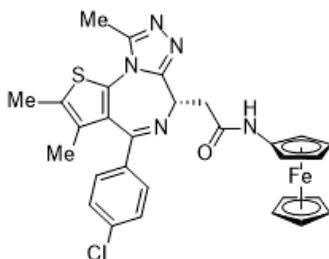
Data collection and refinement statistics are summarized in Table S1. The model and structure factors were deposited in the Protein Data Bank (PDB) under accession number 6SE4.

(+)-JQ-1-OH



A mixture of (+)-JQ-1 (200 mg, 0.438 mmol) and anhydrous DCM (50 mL) was cooled to 0 °C. To the mixture was added dropwise trifluoroacetic acid (20 mL) and the resulting mixture was warmed to ambient temperature and stirred for 16 h under an argon atmosphere. The reaction was concentrated under reduced pressure and to the residue was added a 1:1 mixture of DCM:Et₂O. The solvent was removed under reduced pressure and the sequence repeated five times to give (+)-JQ-1-OH as a yellow solid of sufficient purity to be utilised in subsequent reactions without further manipulation.

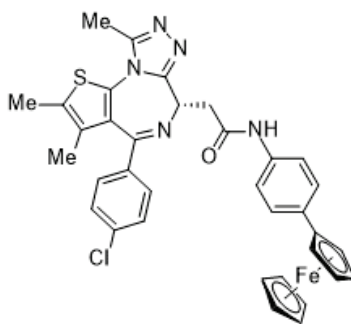
(+)-JD-1



To (+)-JQ-1-OH (176 mg, 0.438 mmol) was added anhydrous THF (20 mL) and anhydrous DIPEA (153 μ L, 0.876 mmol) under an argon atmosphere. To the resulting mixture was added HBTU (332 mg, 0.876 mmol) and aminoferrocene (176 mg, 0.876 mmol) and the mixture stirred at ambient temperature for 16 h. To the mixture was added DCM (50 mL) and a solution of 2M aqueous NaOH (25 mL). The biphasic mixture was separated and the resulting organic extract washed with a solution of 2M HCl (25 mL) followed by brine (25 mL), dried over anhydrous MgSO₄, filtered, and concentrated under reduced pressure to give a brown solid (340 mg). The resulting residue was purified by automated flash column chromatography (EtOAc/MeOH, 100:0 – 90:10, 45 g SiO₂). The appropriate fractions were combined and concentrated under reduced pressure to give (+)-JD-1 as a dark yellow solid (205 mg, 80% over two steps). LCMS (UV, ESI) R_t = 21.07 min, [M+H]⁺ m/z = 583.0, 100% purity. ¹H NMR (600 MHz, *d*₆-DMSO): δ = 9.67 (1H,

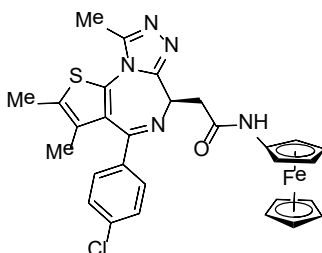
s), 7.51-7.46 (4H, m), 4.63 (1H, m), 4.60-4.55 (2H, m), 4.11 (5H, s), 3.97-3.94 (2H, m), 3.36-3.31 (2H, m), 2.61 (3H, s), 2.42 (3H, s), 1.64 (3H, s). ^{13}C NMR (151 MHz, d_6 -DMSO): δ = 168.1, 163.2, 155.1, 149.8, 130.79, 130.2, 129.8, 129.6, 128.5, 95.4, 68.8, 63.8, 60.9, 60.4, 54.0, 14.1, 12.7, 11.3. HRMS (ESI[M+H⁺]) m/z : Calcd for $\text{C}_{29}\text{H}_{26}\text{ClFeN}_5\text{OS}$ 583.0891; Found 583.0907. $[\alpha]_{\text{D}} = +11.2$ ($t = 24.7$ °C, $c = 1.00$ in MeOH). Enantiomeric excess (ee) = 100% ee by chiral HPLC.

(+)-JD-2



To (+)-JQ-1-OH (88 mg, 0.218 mmol) was added anhydrous THF (10 mL) and anhydrous DIPEA (79 μL , 0.436 mmol) under an argon atmosphere. To the resulting mixture was added HBTU (166 mg, 0.436 mmol) and 4-(aminophenyl)ferrocene (121 mg, 0.436 mmol) and the mixture stirred at ambient temperature for 24 h. To the mixture was added EtOAc (25 mL) and water (25 mL) and the resulting biphasic mixture separated. The aqueous phase was extracted with EtOAc (2 x 25 mL) and the combined organic extracts washed with brine (50 mL), dried over anhydrous MgSO_4 , filtered, and concentrated under reduced pressure to give a brown gum (600 mg). The resulting residue was purified by automated flash column chromatography (EtOAc/MeOH, 100:0 – 85:15, 40 g SiO_2). The appropriate fractions were combined and concentrated under reduced pressure to give (+)-JD-2 as a light brown solid (119 mg, 83%). LCMS (UV, ESI) $R_t = 25.37$ min, $[\text{M}+\text{H}]^+ m/z = 659.0$, 100% purity. ^1H NMR (600 MHz, d_6 -DMSO): δ = 10.31 (1H, s), 7.58 (2H, d, $J = 8.4$ Hz), 7.50-7.46 (4H, m), 7.44 (2H, d, $J = 8.3$ Hz), 4.74-4.72 (2H, m), 4.62 (1H, t, $J = 7.1$ Hz), 4.32-4.29 (2H, m), 4.01 (5H, s), 3.52 (2H, d, $J = 7.1$ Hz), 2.61 (3H, s), 2.42 (3H, s), 1.64 (3H, s). ^{13}C NMR (151 MHz, d_6 -DMSO): δ = 168.4, 163.2, 155.1, 149.9, 137.2, 136.7, 135.2, 133.6, 132.3, 130.8, 130.1, 129.9, 129.6, 128.5, 126.1, 119.1, 84.9, 69.3, 68.6, 65.9, 53.8, 14.1, 12.7, 11.3. HRMS (ESI[+H]) m/z : Calcd for $\text{C}_{35}\text{H}_{30}\text{ClFeN}_5\text{OS}$ 659.1204; Found 659.1241. $[\alpha]_{\text{D}} = -20.0$ ($t = 24.5$ °C, $c = 0.50$ in MeOH). Enantiomeric excess (ee) = 100% ee by chiral HPLC.

(-)-JD-1



(-)-JD-1 was synthesised utilising the analogous protocol detailed above starting from (-)-JQ-1 (20 mg, 0.044 mmol) to give (-)-JD-1 as a dark yellow solid (15 mg, 58% over two steps). ¹H NMR and LCMS were in agreement with those reported above. Enantiomeric excess (ee) = 98.9% ee by chiral HPLC.

Acknowledgments

EPSRC (EP/P026990/1) (SHH, JS, FVD, PB), MRC (MR/N010051/1 to PF) and BBSRC (BB/J001201/2 to AC) are acknowledged for funding this research. ACR was supported by a BBSRC EASTBIO Doctoral Training Partnership award (BB/J01446X/1) and Wellcome Trust for Institutional Strategic Support Fund (204816/Z/16/Z). The authors would like to thank Diamond Light Source for beamtime (proposal mx19301), and the staff of beamlines I03 and I04 for assistance with crystal testing and data collection. The SGC is a registered charity (number 1097737) that receives funds from AbbVie, Bayer Pharma AG, Boehringer Ingelheim, Canada Foundation for Innovation, Eshelman Institute for Innovation, Genome Canada, Innovative Medicines Initiative (EU/EFPIA) [ULTRA-DD grant no. 115766], Janssen, Merck KGaA Darmstadt Germany, MSD, Novartis Pharma AG, Ontario Ministry of Economic Development and Innovation, Pfizer, FAPDF, CAPES, CNPq, São Paulo Research Foundation-FAPESP, Takeda, and Wellcome [106169/ZZ14/Z].

Author contributions: JS, PB, AC, FvD, BN were involved in the overall study design and data analysis. Synthesis was carried out by SHH, JD, CO. BRD assays were carried out and analyzed by AR, OF, AC, PB. Cell-based assays were performed by EL, HJS, TJC, SM, protein purification and X-ray crystallography were performed by TK, SP, PF, F vD, HM, RF, GM, RB were responsible for ee measurements, ADME Tox was performed by MW, CA. JS wrote the manuscript with contributions from SHH, EL, AR, CO, BN, SP and PF. All authors offered critical comments.

Conflicts of Interest

The authors declare no competing financial interests.

Supporting Information. Experimental details including scanned NMR spectra, xray table, chiral HPLC, biological data for the new compounds.

Notes and references

- (1) Ali, I.; Conrad, R. J.; Verdin, E.; Ott, M. Lysine Acetylation Goes Global: From Epigenetics to Metabolism and Therapeutics. *Chem. Rev.* **2018**, *118* (3), 1216–1252. <https://doi.org/10.1021/acs.chemrev.7b00181>.
- (2) Perez-Salvia, M.; Esteller, M. Bromodomain Inhibitors and Cancer Therapy : From Structures to Applications. *Epigenetics* **2017**, *12* (5), 323–339.
- (3) Zaware, N.; Zhou, M. ScienceDirect Chemical Modulators for Epigenome Reader Domains as Emerging Epigenetic Therapies for Cancer and Inflammation. *Curr. Opin. Chem. Biol.* **2017**, *39*, 116–125. <https://doi.org/10.1016/j.cbpa.2017.06.012>.
- (4) Klein, K. Bromodomain Protein Inhibition : A Novel Therapeutic Strategy in Rheumatic Diseases. *Rheum. Musculoskelet. Dis.* **2018**, 1–10. <https://doi.org/10.1136/rmdopen-2018-000744>.
- (5) Noguchi-yachide, T. Review. *Chem. Pharm. Bull. Japan* **2016**, *64* (6), 540–547.
- (6) Muller, S.; Knapp, S. Discovery of BET Bromodomain Inhibitors and Their Role in Target Validation. *Medchemcomm* **2014**, 288–296. <https://doi.org/10.1039/c3md00291h>.
- (7) Muller, S.; Filippakopoulos, P.; Knapp, S. Bromodomains as Therapeutic Targets. *Expert Rev. Mol. Med.* **2011**, *13* (e29), 1–21. <https://doi.org/10.1017/S1462399411001992>.
- (8) Filippakopoulos, P.; Qi, J.; Picaud, S.; Shen, Y.; Smith, W. B.; Morse, E. M.; Keates, T.; Hickman, T. T.; Felletar, I.; Munro, S.; et al. Selective Inhibition of BET Bromodomains. *Nature* **2011**, *468* (7327), 1067–1073. <https://doi.org/10.1038/nature09504>. Selective.
- (9) Alqahtani, A.; Choucair, K.; Ashraf, M.; Hammouda, D. M. Bromodomain and Extra-Terminal Motif Inhibitors : A Review of Preclinical and Clinical Advances in Cancer Therapy. *Futur. Sci. OA* **2019**, *5* (3), FSO372.
- (10) Duan, Y.; Guan, Y.; Qin, W.; Zhai, X. Targeting Brd4 for Cancer Therapy : Inhibitors and Degradable. *Medchemcomm* **2018**, *9*, 1779–1802. <https://doi.org/10.1039/C8MD00198G>.
- (11) Patra, M.; Gasser, G. The Medicinal Chemistry of Ferrocene. *Nat. Rev. Chem.* **2017**, *1*,

0066.

- (12) Gasser, G.; Ott, I.; Metzler-nolte, N. Organometallic Anticancer Compounds. *J. Med. Chem.* **2011**, *54*, 3–25. <https://doi.org/10.1021/jm100020w>.
- (13) Kilpin, K. J.; Dyson, P. J. Enzyme Inhibition by Metal Complexes: Concepts, Strategies and Applications. *Chem. Sci.* **2013**, *41* (0), 1410–1419. <https://doi.org/10.1039/c3sc22349c>.
- (14) Wähler, K.; Kräling, K.; Steuber, H.; Meggers, E. Non-ATP-Mimetic Organometallic Protein Kinase Inhibitor. *ChemistryOpen* **2013**, No. 2, 180–185. <https://doi.org/10.1002/open.201300031>.
- (15) Fujii, S. MedChemComm Expanding the Chemical Space of Hydrophobic Pharmacophores : The Role of Hydrophobic. *Medchemcomm* **2016**, *7*, 1082–1092. <https://doi.org/10.1039/c6md00012f>.
- (16) Spencer, J.; Amin, J.; Coxhead, P.; McGeehan, J.; Richards, C. J.; Tizzard, G. J.; Coles, S. J.; Bingham, J. P.; Hartley, J. A.; Feng, L.; et al. Size Does Matter. Sterically Demanding Metallocene-Substituted 3-Methylidene-Oxindoles Exhibit Poor Kinase Inhibitory Action. *Organometallics* **2011**, *30* (11), 3177–3181. <https://doi.org/10.1021/om200278j>.
- (17) Meggers, E. Targeting Proteins with Metal Complexes. *Chem. Commun.* **2009**, 1001–1010. <https://doi.org/10.1039/b813568a>.
- (18) Allardyce, C. S.; Dyson, P. J. Metal-Based Drugs That Break the Rules. *Dalt. Trans.* **2016**, *45*, 3201–3209. <https://doi.org/10.1039/c5dt03919c>.
- (19) Wu, B.; Ong, M. S.; Groessl, M.; Adhireksan, Z.; Hartinger, C. G.; Dyson, P. J.; Davey, C. A. A Ruthenium Antimetastasis Agent Forms Specific Histone Protein Adducts in the Nucleosome Core. *Chem. - A Eur. J.* **2011**, *17*, 3562–3566. <https://doi.org/10.1002/chem.201100298>.
- (20) Ma, S. D.; Cai, Z.; Wang, H. D.; Leung, C. An Iridium(III)-Based Irreversible Protein–Protein Interaction Inhibitor of BRD4 as a Potent Anticancer Agent. *Chem. Sci.* **2015**, *6*, 5400–5408. <https://doi.org/10.1039/c5sc02321a>.
- (21) Jaouen, G.; Vessieres, A.; Top, S. Chem Soc Rev. *Chem. Soc* **2015**, *44*, 8802–8817. <https://doi.org/10.1039/C5CS00486A>.
- (22) Dive, D.; Biot, C. Ferrocene Conjugates of Chloroquine and Other Antimalarials : The Development of Ferroquine , a New Antimalarial. *ChemMedChem* **2008**, *3*, 383–391. <https://doi.org/10.1002/cmdc.200700127>.
- (23) Plaz, D.; Wieczorek, A.; Ciszewski, W. M.; Kowalczyk, K.; Błauz, A.; Pawledzio, S.; Makal,

- A.; Eurtivong, C.; Arabshahi, H. J.; Reynisson, J.; et al. Synthesis and in Vitro Biological Evaluation of Ferrocenyl Side-Chain-Functionalized Paclitaxel Derivatives. *ChemMedChem* **2017**, *12*, 1882–1892. <https://doi.org/10.1002/cmdc.201700576>.
- (24) Salmon, A. J.; Williams, M. L.; Hofmann, A.; Poulsen, S. ChemComm Protein Crystal Structures with Ferrocene and Ruthenocene-Based Enzyme Inhibitors W. **2012**, 2328–2330. <https://doi.org/10.1039/c2cc15625c>.
- (25) Spencer, J.; Amin, J.; Wang, M.; Packham, G.; Alwi, S. S. S.; Tizzard, G. J.; Coles, S. J.; Paranal, R. M.; Bradner, J. E.; Heightman, T. D. Synthesis and Biological Evaluation of JAHAs : Ferrocene-Based Histone Deacetylase Inhibitors. *ACS Med. Chem. Lett.* **2011**, *2*, 358–362.
- (26) Spencer, J.; Amin, J.; Boddiboyena, R.; Packham, G.; Cavell, B. E.; Syed Alwi, S. S.; Paranal, R. M.; Heightman, T. D.; Wang, M.; Marsden, B.; et al. Click JAHAs: Conformationally Restricted Ferrocene-Based Histone Deacetylase Inhibitors. *Medchemcomm* **2012**, *3* (1), 61–64. <https://doi.org/10.1039/c1md00203a>.
- (27) Sansook, S.; Tuo, W.; Lemaire, L.; Tourteau, A.; Barczyk, A.; Dezitter, X.; Klupsch, F.; Leleu-Chavain, N.; Tizzard, G. J.; Coles, S. J.; et al. Synthesis of Bioorganometallic Nanomolar-Potent CB2agonists Containing a Ferrocene Unit. *Organometallics* **2016**, *35* (19), 3361–3368. <https://doi.org/10.1021/acs.organomet.6b00575>.
- (28) Anders, L.; Guenther, M. G.; Qi, J.; Fan, Z. P.; Marineau, J. J.; Rahl, B.; Lovén, J.; Sigova, A. A.; Smith, W. B.; Lee, T. I.; et al. Genome-Wide Determination of Drug Localization. *Nat. Biotechnol.* **2014**, *32* (1), 92–96. <https://doi.org/10.1038/nbt.2776>. Genome-wide.
- (29) Runcie, A. C.; Zengerle, M.; Chan, K.-H.; Testa, A.; van Beurden, L.; Baud, M. G. J.; Epemolu, O.; Ellis, L. C. J.; Read, K. D.; Coulthard, V.; et al. Chemical Science Allele-Selective BET Bromodomain Inhibition †. *Chem. Sci.* **2018**, *9*, 2452–2468. <https://doi.org/10.1039/C7SC02536J>.
- (30) Roberts, J. M.; Bradner, J. E. HHS Public Access. *Curr. Protoc. Chem. Biol.* **2016**, *7* (4), 263–278. <https://doi.org/10.1002/9780470559277.ch150024.A>.
- (31) Baud, M. G. J.; Lin-shiao, E.; Cardote, T.; Tallant, C.; Pschibul, A.; Chan, K.; Zengerle, M.; Garcia, J. R.; Terence, T.; Ferguson, F. M.; et al. A Bump-and-Hole Approach to Engineer Controlled Selectivity of BET Bromodomain Chemical Probes. *Science* (80-.). **2015**, *346* (6209), 638–641. <https://doi.org/10.1126/science.1249830.A>.
- (32) Baud, M. G. J.; Lin-Shiao, E.; Zengerle, M.; Tallant, C.; Ciulli, A. New Synthetic Routes to Triazolo-Benzodiazepine Analogues: Expanding the Scope of the Bump-and-Hole Approach for Selective Bromo and Extra-Terminal (BET) Bromodomain Inhibition. *J. Med.*

- Chem.* **2016**, *5* (59), 1492–1500. <https://doi.org/10.1021/acs.jmedchem.5b01135>.
- (33) Ocasio, C. A.; Sansook, S.; Jones, R.; Roberts, J. M.; Scott, T. G.; Tsoureas, N.; Coxhead, P.; Guille, M.; Tizzard, G. J.; Coles, S. J.; et al. Pojamide: An HDAC3-Selective Ferrocene Analogue with Remarkably Enhanced Redox-Triggered Ferrocenium Activity in Cells. *Organometallics* **2017**, *36* (17), 3276–3283. <https://doi.org/10.1021/acs.organomet.7b00437>.
- (34) Delmore, J. E.; Issa, G. C.; Lemieux, M. E.; Rahl, P. B.; Shi, J.; Jacobs, H. M.; Kastritis, E.; Gilpatrick, T.; Paranal, R. M.; Qi, J.; et al. BET Bromodomain Inhibition as a Therapeutic Strategy to Target C-Myc. *Cell* **2011**, *146* (6), 904–917. <https://doi.org/10.1016/j.cell.2011.08.017>.
- (35) Pluripotency, S. C.; Suppressed, I.; Horne, G. A.; Stewart, H. J. S.; Dickson, J.; Knapp, S.; Ramsahoye, B.; Chevassut, T. Nanog Requires BRD4 to Maintain Murine Embryonic Stem Cell Pluripotency and Is Suppressed by Bromodomain Inhibitor JQ1 Together with Lefty1. *Stem Cells Dev.* **2015**, *24* (7), 879–891. <https://doi.org/10.1089/scd.2014.0302>.
- (36) Gascon, J. M.; Oliveri, V.; McGown, A.; Kaya, E.; Chen, Y.; Austin, C.; Walker, M.; Platt, F. M.; Vecchio, G.; Spencer, J. Synthesis and Study of Multifunctional Cyclodextrin – Deferasirox Hybrids. *ChemMedChem* **2019**, *14*, 1484–1492. <https://doi.org/10.1002/cmdc.201900334>.
- (37) Richard, M.; Hamels, D.; Pigeon, P.; Top, S. Oxidative Metabolism of Ferrocene Analogues of Tamoxifen : Characterization and Antiproliferative Activities of the Metabolites. *ChemMedChem* **2015**, *10*, 981–990. <https://doi.org/10.1002/cmdc.201500075>.
- (38) D'Orchymont, F.; Hess, J.; Panic, G.; Jakubaszek, M.; Gemperle, L.; Keiser, J.; Gasser, G. Drug Mefloquine as New Antischistosomal Drug. *Medchemcomm* **2018**, *9*, 1905–1909. <https://doi.org/10.1039/C8MD00396C>.
- (39) Kabsch, W. Acta Crystallography Section D. *Biol. Crystallogr.* **2010**, 125–132. <https://doi.org/10.1107/S0907444909047337>.
- (40) Murshudov, G. N.; Nicholls, R. A. REFMAC 5 for the Refinement of Macromolecular Crystal Structures Research Papers. *Acta Crystallogr. Sect. D Biol. Crystallogr.* **2011**, *D67*, 355–367. <https://doi.org/10.1107/S0907444911001314>.
- (41) Winter, G. Xia2 : An Expert System for Macromolecular Crystallography Data Reduction. *J. Appl. Crystallogr.* **2010**, *43*, 186–190.
- (42) Winn, M. D.; Charles, C.; Cowtan, K. D.; Dodson, E. J.; Leslie, A. G. W.; McCoy, A.; Stuart, J.; Garib, N.; Powell, H. R.; Randy, J. Overview of the CCP 4 Suite and Current

Developments Research Papers. *Acta Crystallogr. Sect. D Biol. Chem.* **2010**, *D67*, 235–242. <https://doi.org/10.1107/S0907444910045749>.

- (43) Moriarty, N. W.; Grosse-Kunstleve, Ralf, W.; Adams, Paul, D. Electronic Ligand Builder and Optimization Workbench (ELBOW): A Tool for Ligand Coordinate and Restraint Generation Research Papers. *Acta Crystallogr. Sect. D Biol. Crystallogr.* **2009**, No. D65, 1074–1080. <https://doi.org/10.1107/S0907444909029436>.
- (44) Emsley, P.; Lohkamp, B. Features and Development of Coot Research Papers. *Acta Crystallogr. Sect. D Biol. Crystallogr.* **2010**, *D66*, 486–501. <https://doi.org/10.1107/S0907444910007493>.